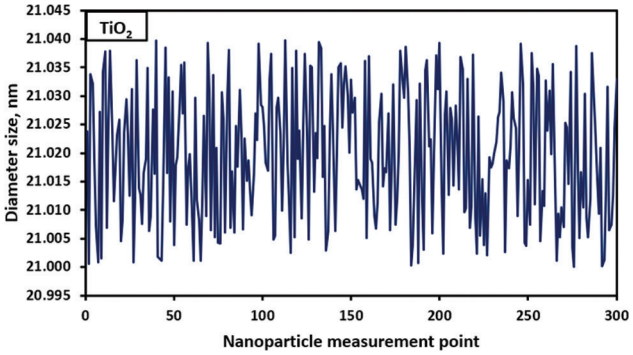

Figure 3. TiO_2 Nanoparticles diameter size distribution.

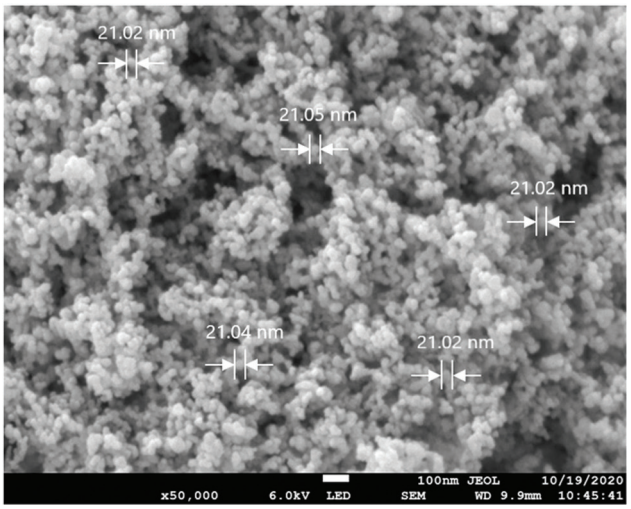

Figure 4. TiO_2 Nanoparticles morphology in 50,000 magnifications.

stability of the TiO_2-POE nanolubricant. These three assessments are linked together as done by previous researchers [23-25]. The goal of visual assessment is to detect the sedimentation and agglomeration of the formed nanolubricant visually. Ultraviolet-visible spectroscopy will be used to confirm the results of the visual examination. The absorbance ratio of the nanolubricant that was measured on the first day when the nanolubricant was synthesized is used to persuade the value of Ultraviolet-visible spectroscopy. The absorbance ratio was measured over 360 hours. The absolute zeta potential assessment results will confirm the highest absorbance ratio value results, as noted by Graves et al. [26].

Statistical Analysis of Data and Optimization Process

All of the tests were done three times, and the outcomes were recorded as mean amount. The experimental design's independent variables were optimized and evaluated using Design-Expert software. The model was statistically analyzed using the analysis of variance method (ANOVA). The R^2 coefficient and the adjusted R^2 coefficient were used to assess the superiority of the fit of the polynomial model equivalence, and the numerical and regression coefficient significance was validated using the F-test and p-value, respectively [27, 28].

The optimization procedure determines which sample has the best or most optimal value. In this study, the optimal parameter in the optimization process is to maximize the response in the form of the absorbance ratio of the components influencing the response. The goal of figuring out this optimization is to help reduce the number of experiments while increasing the response output [29].

RESULT AND DISCUSSION

TiO_2 Nanoparticle Characterization

Field Emission Scanning Electron Microscopy (FESEM) was employed to characterize TiO_2 nanoparticles. FESEM JSM-7800F from JEOL Ltd was used to confirm the physiology, dimension, and form of TiO_2 nanoparticles. The graph was acquired with a magnification setting of 50,000x and an LED mode of 7.0 kV. Particle size analysis was performed using Image J software, which was utilized to evaluate and validate the nanoparticle distribution over all ranges and average diameters as suggested by previous researchers [30-33].

Figure 4 depicts the diameter distribution of TiO_2 nanoparticles. TiO_2 nanoparticles have an average grain size of 21.12 nm, according to the data. This finding matches the manufacturer's specification. Figure 1 displays a FESEM image of dry TiO_2 nanoparticles supplied by the manufacturer, illustrating the distribution and morphology of the nanoparticles. The particles are spherical. As can be observed, the particles are in the shape of aggregates or agglomerates. These agglomerates or agglomerates must be broken down during the nanolubricant processing to achieve a stable nanolubricant. The stability of TiO_2-POE nanolubricant will be discussed in depth in the following section.

TiO_2-POE Nanolubricant Visual Analysis

The first step in verifying the stability of TiO_2-POE nanolubricant is a visual examination. The findings of 720 hours of observations are depicted in Figure 5. The first visible observations were made on the first day of making the nanolubricant, and the last visual observations were made on day 30. Figure 5(a) depicts the nanolubricant after it had been prepared on the observation tube. The six nanolubricant tubes, from left to right, exhibit nanolubricant samples that were sonicated for 0, 40, 60, 80, 100, and 120 min. All of the samples had equally distributed nanoparticles in the POE lubricant. There was no evidence of agglomeration or sedimentation in any of the samples at this stage. This phenomenon suggests that each sample has generated nanolubricant homogeneity.

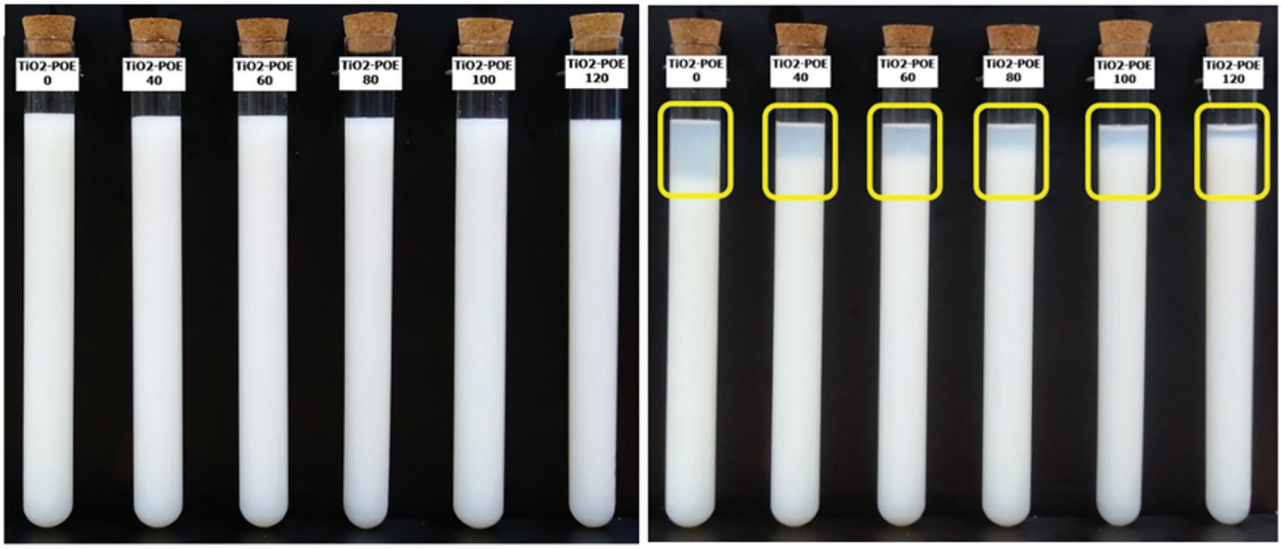

Figure 5. TiO_2-POE nanolubricant visual observation comparison (a) day 1 and (b) day 30.

Figure 5(b) shows the results of observations on day 30 after the nanolubricant had been in the observation tube for 720 hours. The nanolubricant sample that was not subjected to sonication suffered more damage, as demonstrated by sedimentation at the observation tube, as shown in yellow square in the figure. This phenomenon suggests that the nanolubricant is agglomerated to a great degree. The aggregation of the nanolubricant will facilitate sedimentation, as reported by Sharif et al. [34]. Two primary causative variables cause this phenomenon. The van der Waals force, which promotes amplification between nanoparticle molecules, is the first factor. The second factor is the concentration of the nano powder, which is superior than that of the lubricant, leading the nanoparticles to always fall to the tube's bottom due to gravitational forces. The sedimentation process in the nanolubricant sample will be accelerated due to the augmentation of these nanoparticles, as noted by Ali et al. [35].

The second sample was the one that was subjected to a 40-min sonication treatment. Although there is a significant drop in this sample, it is still apparent that part of the nanolubricant near the tube's bottom is in a more stable state. The sonication effect is responsible for this phenomenon. Nanoparticle particles break apart and run apart as they are augmented and clustered together, breaking their ties. The higher the level of augmentation in the nanolubricant, the greater the agglomeration that happens, putting the nanolubricant's sedimentation obvious visually.

The TiO_2-POE 0 graph, as shown in Figure 6(a), is a nanolubricant sample that has not been subjected to a sonication process. The wave spectral has fluctuated along the wavelength since the scanning measurement commencement. This finding demonstrates that agglomeration is widespread across the nanolubricant region. Figure 6(b) shows the same result, with no decrease in agglomeration but an increase in the number of graph spectrums. At the 410 nm wavelength, the comparison between absorbance measurements on the 1st and 30th days was determined.

TiO_2-POE Nanolubricant Absorbance Analysis

The amount of light that the sample can absorb in the cell cuvette is quantified by absorbance. The density of the nanolubricant sample is closely connected to absorbance. Technically, the light source emits a specified amount of UV light throughout the sample. The sample absorbs the light in the cell cuvette, and the results of the light absorption measurement with absorbance units will be presented on display.

A 3 ml sample of TiO_2-POE nanolubricant was inserted in each quartz cuvette cell for this experiment. In addition, the cuvette cell sample is inserted into the UV visible spectrophotometry slot, which has a measuring range of 1000-200 nm. When comparing the absorbance measurement findings from day 1 to day 30, it can be seen that all samples have a declining trend, as formerly done by Nugroho et al. [19] and Hou et al. [36]. The sample's comparison point is taken at 410nm, where a significant absorbance level has been attained by marking the curve's height on the graph of the absorbance measurement findings in all samples.

Figure 6 depicts the absorbance measurement results for all samples evaluated on day 1 and day 30. Both images indicate that UV light has efficiently absorbed the nanoparticles in the nanolubricant sample using UV visible spectrophotometry. This phenomenon is demonstrated by the findings of the scanning spectrum from 300-1000 nm. The two plots show several oscillating spectrum peaks. The peak

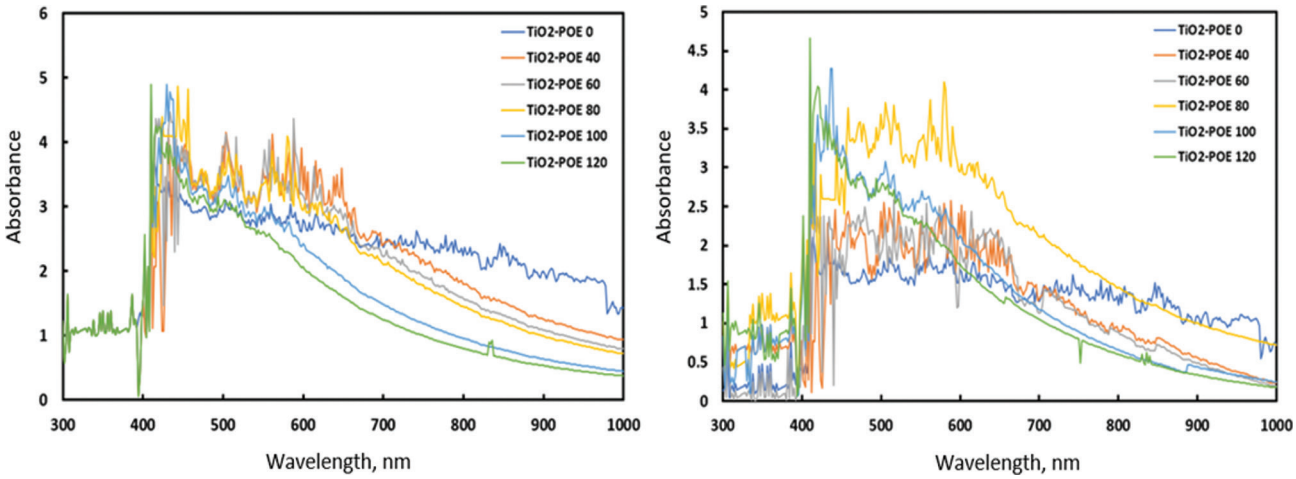

Figure 6. TiO_2-POE nanolubricant absorbance value comparison (a) day 1 and (b) day 30 from all samples.

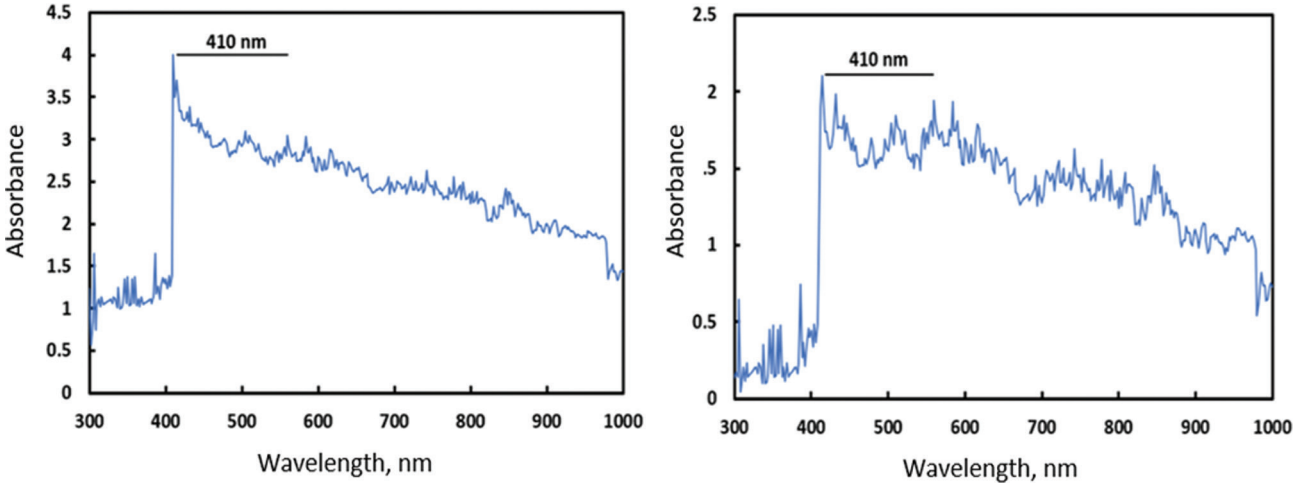

Figure 7. TiO_2-POE nanolubricant absorbance value comparison (a) day 1 and (b) day 30 from sample 1 with 0 min ultrasonication treatment.

of the spectrum depicts the addition of nanoparticles to the nanolubricant. The addition of nanoparticles to the nanolubricant sample promotes the production of agglomerates. Figures 6(a) and 6(b) show that nanoparticle augmentation is expanding in all samples. The increasing number of spectral peaks evidences this.

$$\bar{A}_r = \frac{A}{A_0} \tag{2}$$

The comparison of absorbance values in sample 1 is shown in Figure 7. The nanolubricant in sample 1 was made using simply a magnetic stirrer for 30 min, with no ultrasonication treatment. Figure 7(a) shows that, despite the nanolubricant being just prepared, several nanoparticle augmentations can be observed clearly from 1000 to 300 nm. The augmentation of nanoparticles is still visible and increases up to the point of 410 nm. There is a significant drop following that, followed by the same nanoparticle enhancement as before. Because the nanoparticles are not entirely dispersed in the lubricant, nanoparticle augmentation occurs in all regions of the lubricant [37].

The nanoparticles' Van der Walls force leads the TiO_2 nanoparticles to link together. The dipoles of the TiO_2 nanoparticle molecules provide the Van der Waals force for this nanolubricant. The electron distribution in the molecule creates the dipole. Molecules with high concentration levels become negative dipoles, allowing them to attract molecules with low concentration levels, such as molecules with positive dipoles and non-charged dipoles. This process

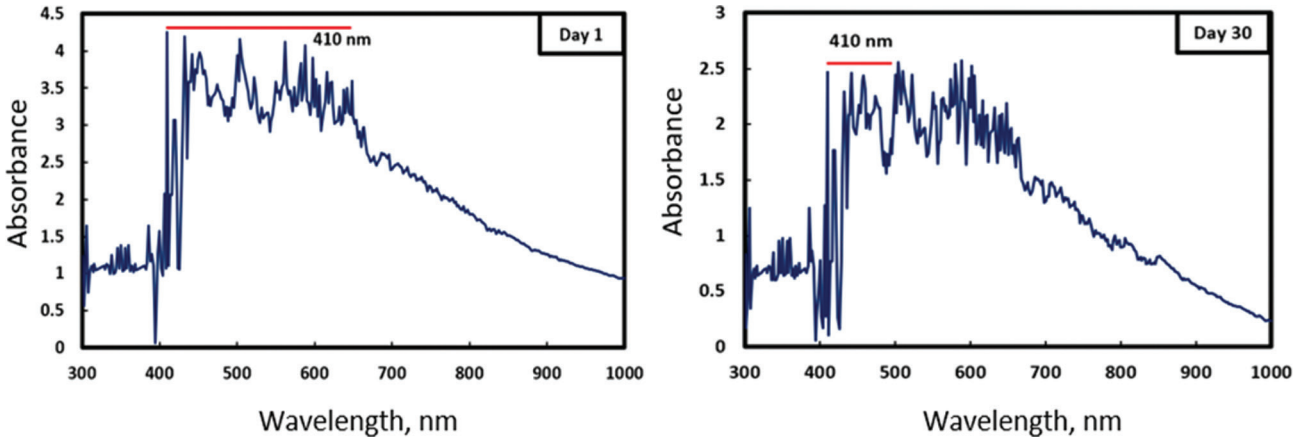

Figure 8. TiO_2-POE nanolubricant absorbance value comparison (a) day 1 and (b) day 30 from sample 2 with 40 min ultrasonication treatment.

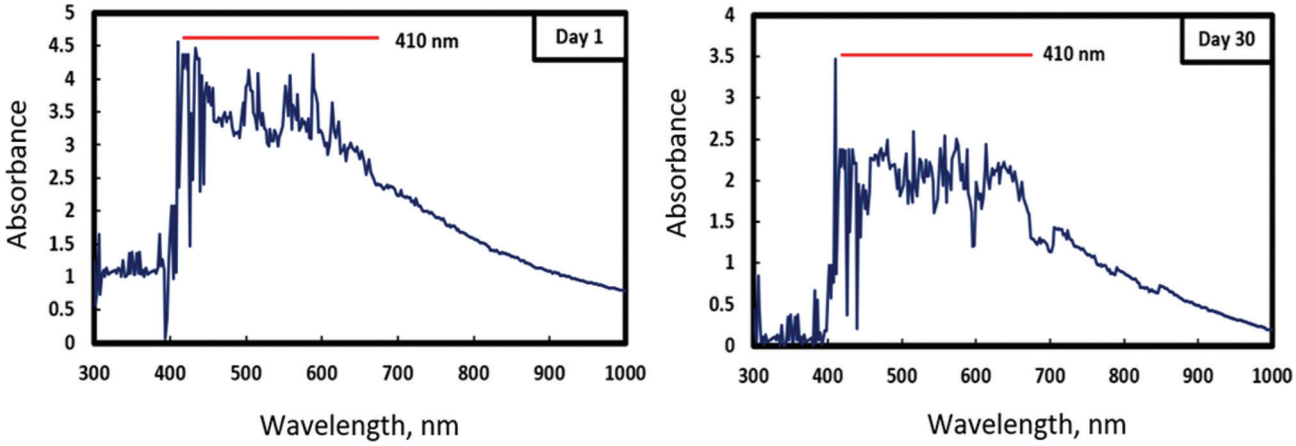

Figure 9. TiO_2-POE nanolubricant absorbance value comparison (a) day 1 and (b) day 30 from sample 3 with 60 min ultrasonication treatment.

is ongoing in the nanolubricant area, which contains the nanoparticles. As a result, the Van der Waals effect can be defined as the fusion of multiple nanoparticle molecules, resulting in an agglomeration as investigated by Tiwari et al. [38] and Sarsam et al. [39].

The 410 nm point was used as a reference to measure the rate of reduction in the absorbance value over time, as shown in Figure 7. The absorbance ratio value may be calculated based on this observation to estimate the stability level of TiO_2-POE nanolubricant as suggested by Zawawi et al. [40]. The initial absorbance (A) is compared to the final absorbance (A_o) produced by equation 2 to determine the absorbance ratio ($\bar{A}_r$). Figures 8, 9, 10, and 11 show the effect of ultrasonication duration on the absorbance value of samples 2, 3, 4, and 5 after ultrasonication treatment for 40, 60, 80, and 100 min, respectively. In general, absorbance values on the 30th day are decreasing when compared to the first day. This decrease is due to the formation of agglomerates from aggregated nanoparticles. The agglomeration's gravitational force promotes the sedimentation of the nanolubricant.

Figure 11 compares the absorbance values of sample 6 on day 1 and day 30. On the first day, the nanoparticles were well dispersed in the lubricant. The spectrum begins to fluctuate around 550 nm and reaches its highest peak point at 410 nm with a value of 4,905 in Figure 11(a). The spectral peak at 411 nm drops to 300 nm, a significant decrease. The presence of agglomerates at each spectral peak in the 1000-300 nm region is demonstrated by this phenomenon.

A spectral pattern in Figure 11(b) is comparable to the spectrum pattern on the absorbance data in Figure 11(b). However, the findings of UV visible spectrophotometry tests in Figure 8(b) show agglomeration at multiple spots along the 850-650 nm area, a drop in the spectral peak at

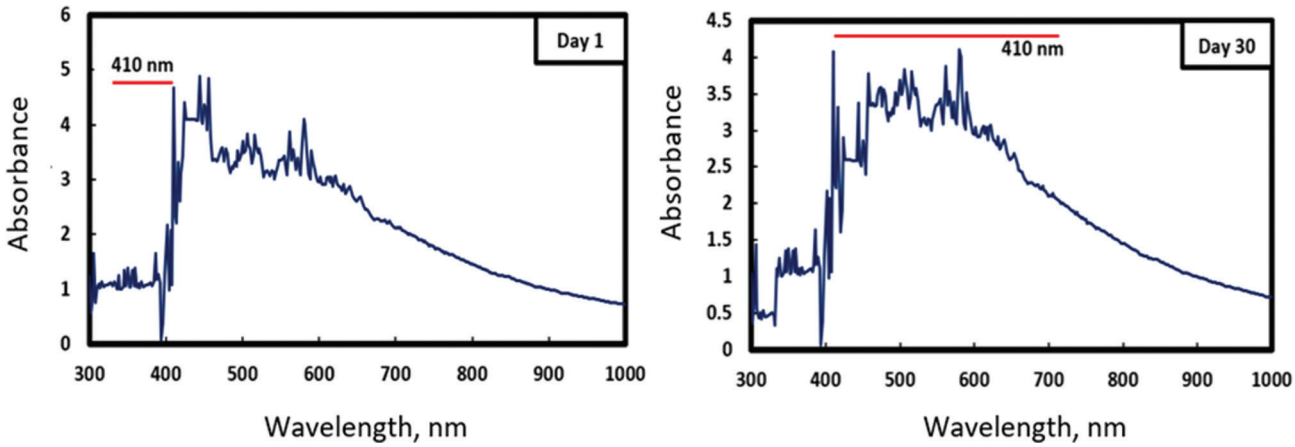

Figure 10. TiO_2-POE nanolubricant absorbance value comparison (a) day 1 and (b) day 30 from sample 4 with 80 min ultrasonication treatment.

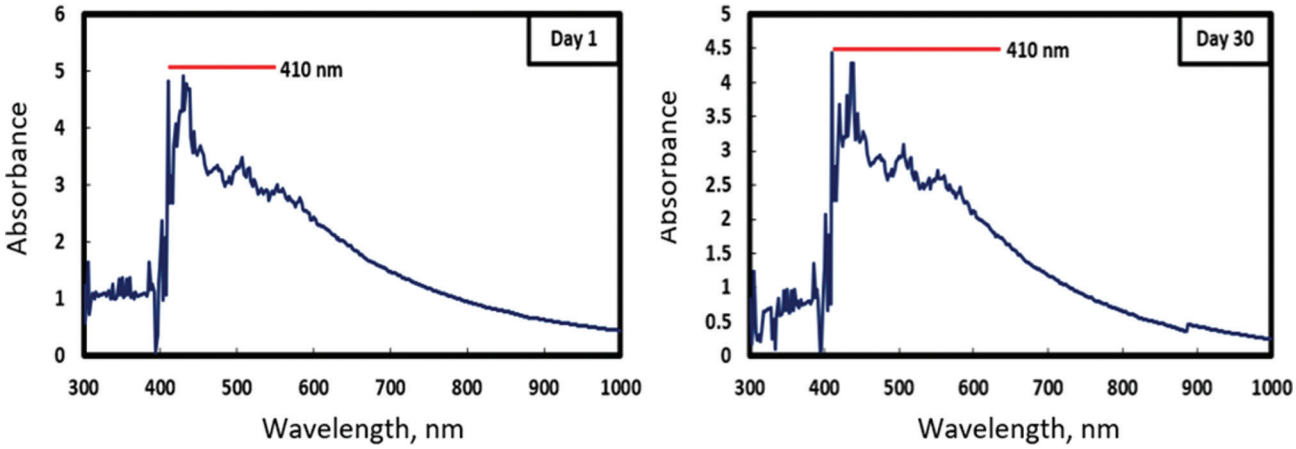

Figure 10. TiO_2-POE nanolubricant absorbance value comparison (a) day 1 and (b) day 30 from sample 5 with 100 min ultrasonication treatment.

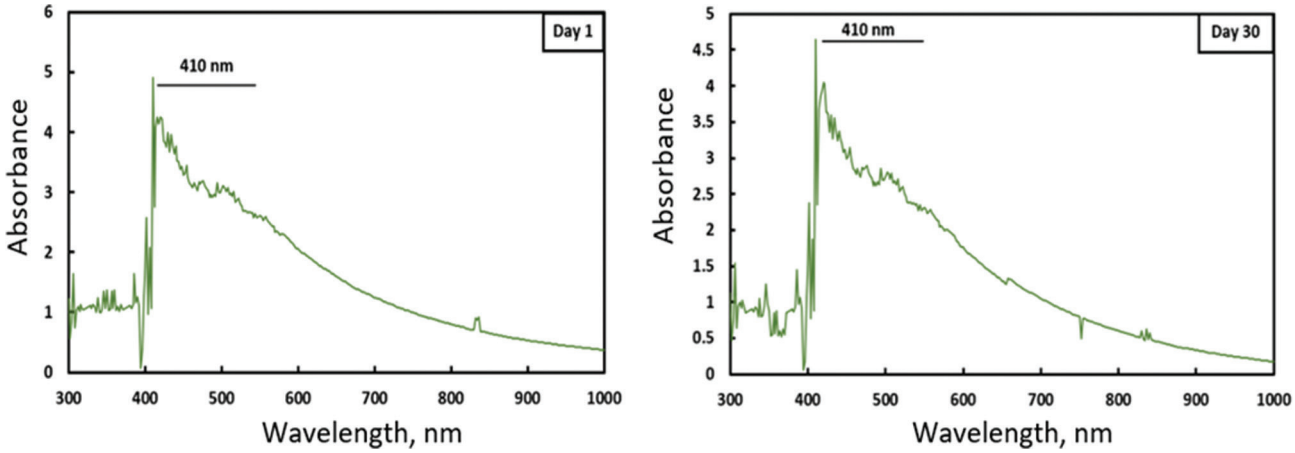

Figure 11. TiO_2-POE nanolubricant absorbance value comparison (a) day 1 and (b) day 30 from sample 6 with 120 min ultrasonication treatment.

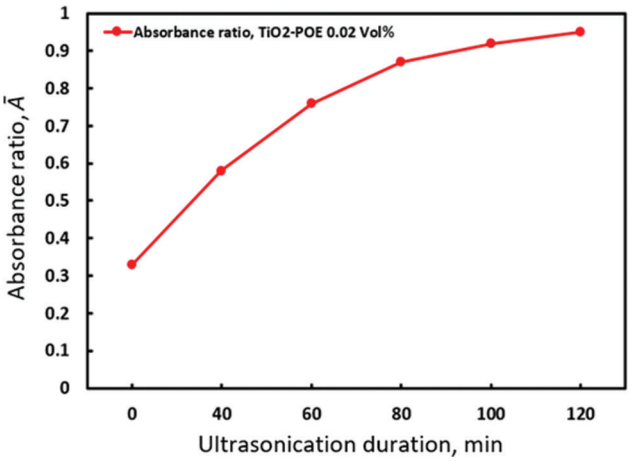

Figure 12. TiO_2-POE nanolubricant absorbance ratio as a dependent of ultrasonication duration.

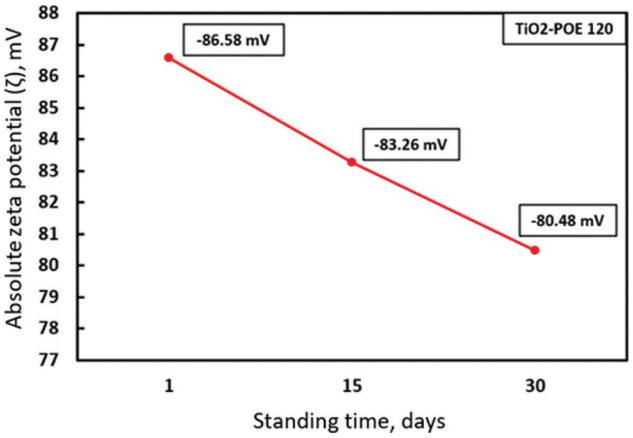

Figure 13. TiO_2-POE nanolubricant absolute zeta potential from sample 6.

410 nm to 4,648 nm, and spectral peaks, which are more volatile in the range of 411 – 300 nm.

This occurrence makes sense because the experiment was conducted on the 30th day when many nanoparticles were augmented and generated agglomeration at multiple nanolubricant regions [41]. Although there were new agglomerations at a few spots and a drop in the spectral peak in the 410 nm area, the absorbance value at that point did not change much. As a result, sample 6 is the one with the most negligible absorbance reduction value.

The duration of the nanolubricant's sonication treatment leads to an increase in the absorbance ratio, as shown in Figure 12. The sampling with the longest sonication period, 120 min, had the most excellent absorbance ratio value, 0.95, whereas the sampling with the shortest sonication period, 100 min, had a slightly lower absorbance ratio value, 0.92. This graph shows how sonication can prevent agglomeration and sedimentation in nanolubricant. As a result, the nanolubricant's stability can be obtained by applying the sonication treatment to the nanolubricant for the appropriate amount of time. The optimum sonication duration for achieving the best level of stability for TiO_2-POE nanolubricant was 120 min in this investigation.

TiO_2-POE Nanolubricant Zeta Potential Analysis

The goal of the zeta potential measurement on TiO_2-POE nanolubricant is to determine the sample's stability. The zeta potential is a significant degree of the stability of the nanolubricant dispersion because it determines the potential variance amid the dispersing medium and the steady fluid layer linked to the dispersed particles.

Figure 13 shows the absolute value of the TiO_2-POE sample's zeta potential after a 120-min ultrasonication treatment. On days 1, 15, and 30, the absolute zeta potential value was -80.48 mV, -83.26 mV, and -80.48 mV, respectively. According to the graph, the absolute zeta potential value decreases as sample storage duration increases. However, the resulting decrease in the absolute value of the zeta potential is modest. Mahbubul et al. [42] noted that nanofluids with an absolute zeta potential of -80.48mV are classed as excellent nanofluids, which have excellent of stability because they are in the -60 to -100 mV range. The surface charge of TiO_2 nano powder s is indicated by the negative absolute zeta potential of TiO_2-POE nanolubricant [43-45].

One Factor at A Time (OFAT)

This OFAT optimization technique aims to discover the optimum factor for the intended response as [46-49]. The parameters and constraints used in the response surface optimization process employing OFAT are indexed in Table 3.

In this investigation, the sonication duration compared to the absorbance ratio value is one measure of the nanolubricant's stability level. The original design type is designed with 11 runs, and this table consists of three primary components that explain the types of tests performed. The next step is to determine the detail factor, the sonication duration, which can range from 40 to 120 min. The absorbance ratio, which ranges from 0.58 to 0.95, is the dependent variable in this study. The absorbance ratio obtained a mean of 1.63793 with a standard deviation of 0.132157 based on the experimental data. The cubic model is the one that OFAT recommends.

Analysis of variance (ANOVA)

The statistical results based on ANOVA are presented in Table 4 and Table 5. The model is significant since it has a p-value of 0.0001, less than 0.05, and an F-value of 1179.53 and 18200.55. The F-value and p-values were also used to determine the significance of each component. The more significant the relevant coefficient term is, the bigger the degree of the F-value and the lower the p-value is. The

Table 3. OFAT outline

Subject	Response surface
Initial design	Quadratic
Runs	11
Factor	Sonication duration
Unit	Min
Low Actual	40.00
High Actual	120.00
Mean	80.00
Std. Dev	25.584
Response	Absorbance ratio
Unit	Abs. unit
Analysis	Polynomial
Min	0.58
Max	0.95
Mean	0.826364
Standard Deviation	0.132157
Model	Cubic

A-sonication time, A^2, and A^3 model terms were significant in this scenario, with F values of 2007.13, 7795.45, and 86.85 for each model as stated in Table 5, respectively.

According to Table 6, the duration of sonication has a substantial impact on the absorbance ratio. This number is confirmed by the correlation coefficient of regression (R^2) of 0.9989 in day 15th and 0.9999 in day 30th, which perfectly agrees with the adjusted R^2 of 0.9983 and 0.9998 respectively. These models have a high level of replication, which ensures that the results are accurate and dependable. A shallow pure error value of 0.000 indicates this.

Figures 14a and 14b show the adequacy of the regression model estimated by residuals and residuals versus predicted plots. The experimental and predictive points are collected near the normality line, as shown in Fig. 14a, confirming the analytical system's consistency. In contrast, as shown in Fig. 14b, is a randomly distributed residue across the baseline with no perceptible trend. Figure 14c. confirms the predicted value's closeness to the true value as reported by [28]. As a result of the three plots, it is possible to conclude that the cubic-square equation model is reliable enough to

Table 4. Analysis of variance (ANOVA) for absorbance ratio in Day 15th

Source	Sum of Squares	df	Mean Square	F value	p-value prob > F	Remark
Model	0.042	2	0.021	1779.53	<0.0001	Significant
A-Sonication Duration	0.041	1	0.041	3471.59	<0.0001	
A^2	1.035E-003	1	1.035E-003	87.46	0.0007	
Residual	4.734E-005	4	1.184E-005			
Lack of Fit	2.239E-005	2	2.367E-005			
Pure Error	0.000	2	0.000			
Car Total	0.042	6				

Table 5. Analysis of variance (ANOVA) for absorbance ratio in Day 30th

Source	Sum of Squares	df	Mean Square	F value	p-value prob > F	Remark
Model	0.17	3	0.058	18200.55	<0.0001	Significant
A-Sonication Duration	6.419E-003	1	6.419E-003	2007.13	<0.0001	
A^2	0.025	1	0.025	7795.45	<0.0001	
A^3	2.778E-004	1	2.778E-004	86.85	0.0005	
Residual	2.239E-005	7	3.198E-006			
Lack of Fit	2.239E-005	1	2.239E-005			
Pure Error	0.000	6	0.000			
Car Total	0.17	10				

Table 6. Coefficient of regression

Parameters	Ultrasonication duration standing time		Wavelength	
	Day 15th	Day 30th	Day 15th	Day 30th
Standard deviation	3.440E-003	1.788E-003	0.036	0.043
Mean	0.89	0.83	0.81	0.72
CV %	0.39	0.22	4.66	5.98
Press	1.340E-004	1.204E-004	0.014	0.021
R-Squared	0.9989	0.9999	0.9155	0.9614
Adjusted R^2	0.9983	0.9998	0.8733	0.9421
Prediction R^2	0.9968	0.9993	0.7696	0.8876
Adequate Precision	84.855	343.091	9.570	14.896

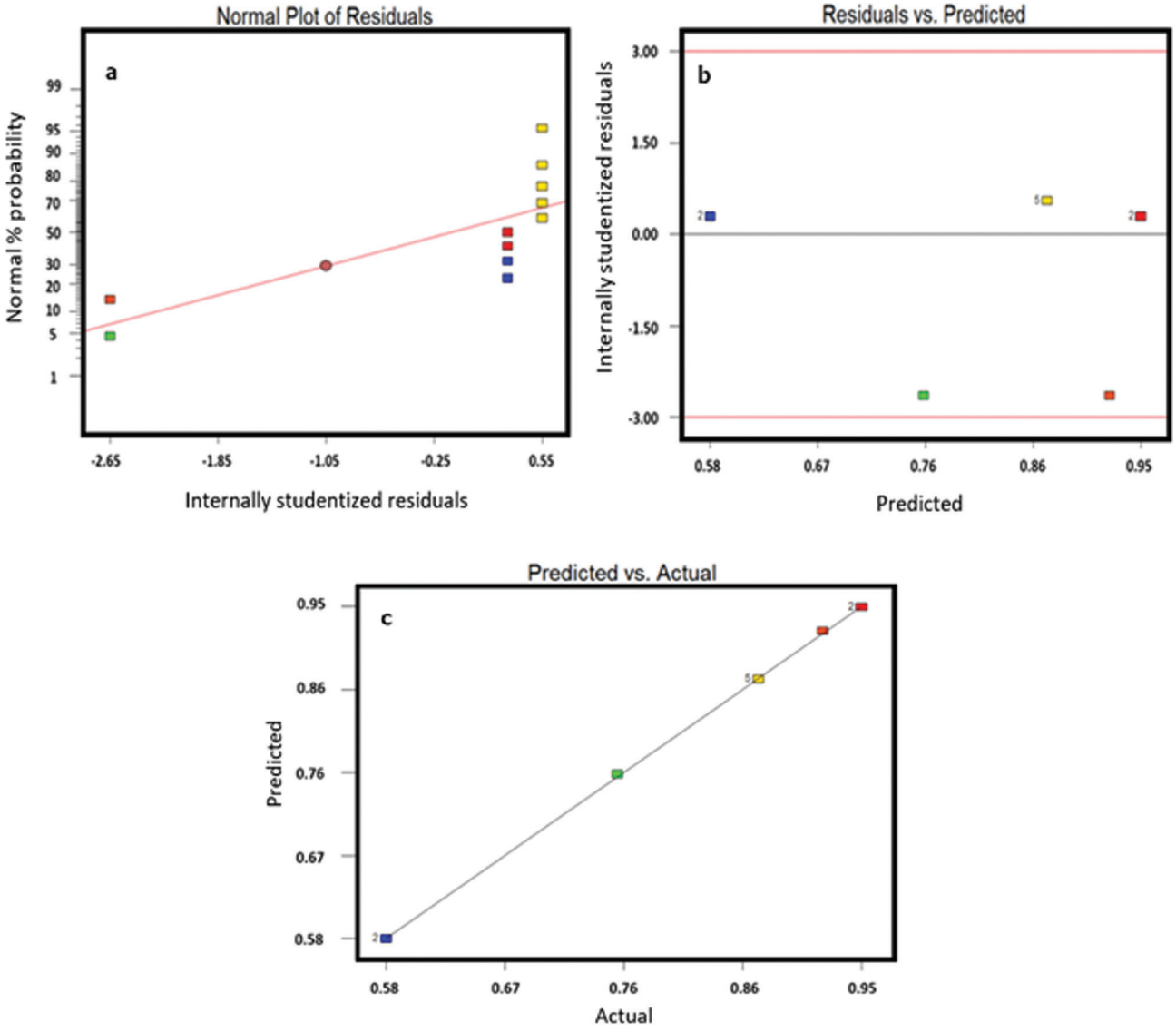

Figure 14. (a) Normal plot of residuals; correlation (b) amid residuals and predicted plot; (c) predicted and the present work findings plot.

establish a relationship between the effect of ultrasonication duration on the absorbance ratio.

R^2 has a high value due to the high accuracy of measurements made during the experimental process. Data measurements were performed three times to ensure the data's level of reliability and consistency, as suggested by Bahiraei et al. [50]. The use of a quartz cuvette allows for repeated data collection on the spectrophotometer without compromising the accuracy of the measurement results. These models are very close to the standing times of 15 and 30 days, demonstrating that the duration of ultrasonication has a significant effect on the absorbance ratio value in each sample. The coefficient of multiple determination (R^2 = 0.9989 and 0.9999 in the absorbance ratio model) and the second value of large R^2 indicate that the cubic model can reflect 99.89% and 99.99% of the total variation, respectively. As reported by Hemmat Esfe et al.[51] and Meybodi et al. [52], R^2 values close to 1 indicate a suitable model

Table 7. Uncertainty

Description	Absorbance ratio		Wavelength	
	Day 15th	Day 30th	Day 15th	Day 30th
Uncertainty	± 0.07	± 0.09	± 0.04	± 0.07

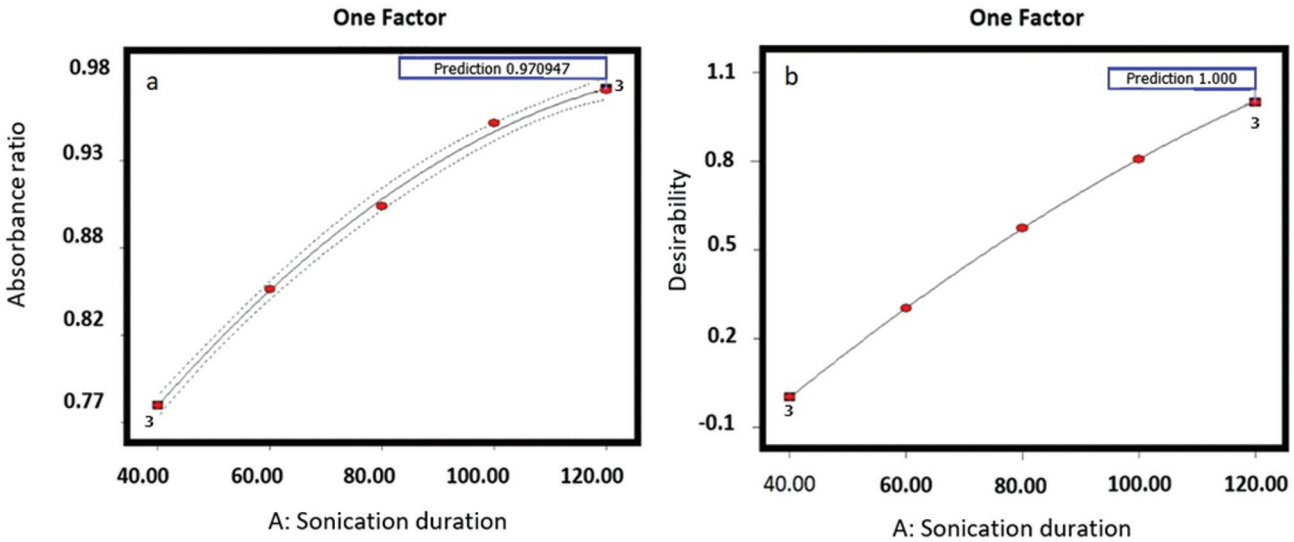

Figure 15. Plot of (a) absorbance ratio as the dependent of sonication and (b) desirability in a one factor at a time in day 15th.

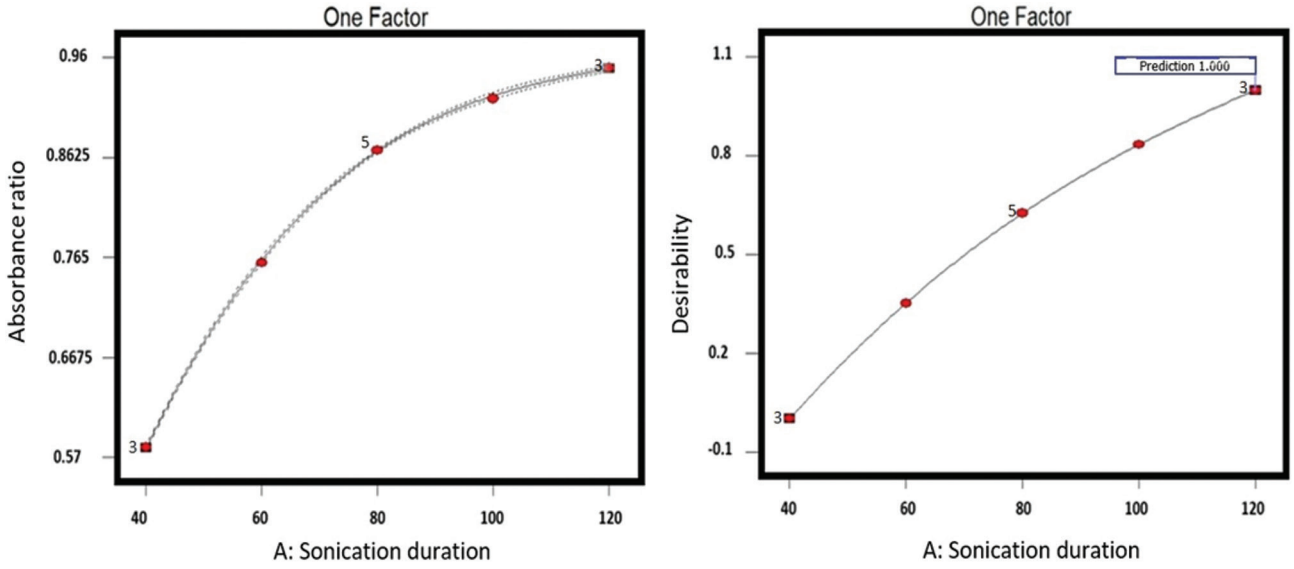

Figure 16. Plot of (a) absorbance ratio as the dependent of sonication and (b) desirability in a one factor at a time in day 30th.

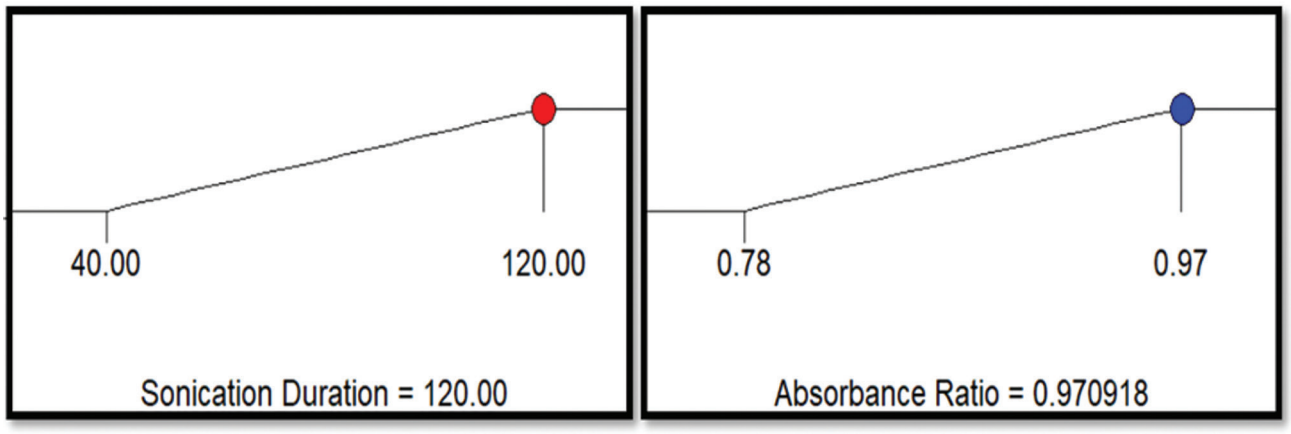

Figure 17. Plot of Ramps plot solution of OFAT in day 15th.

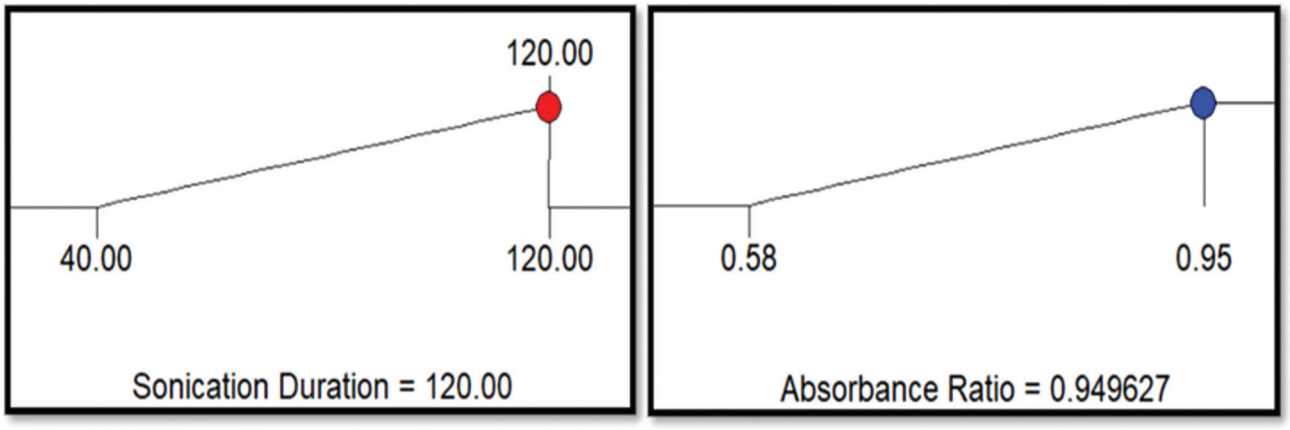

Figure 18. Plot of Ramps plot solution of OFAT in day 30th.

based on reliable and consistent data and very low error. However, the uncertainty has been calculated to quantity the error in this measurement as shows in Table 7.

Solution

Figure 16 (a) depicts the relationship between absorbance ratio and sonication duration. The sonication period of 120 min is the peak point for the maximum absorbance ratio value, as seen in the graph. The absorbance ratio at the sonication duration points of 100 min, on the other hand, is only slightly different from the absorbance ratio at the sonication duration point of 120 min. If the treatment is prolonged for longer than 120 min, the absorbance ratio may begin to decline. The findings are consistent with what has been published in the literature [53-56].

CONCLUSION

Several key points can be concluded based on experimental evaluation and process optimization employing one factor at a time:

Visual inspection, UV Visible spectrophotometry, and zeta potential were adopted to investigate the stability of TiO2-POE in an experimental setting. The outcomes of these three methods all verify each other. Sample 6 has the least amount of sedimentation during 720 hours when compared to the other samples. This result is confirmed by the fact that sample 6 has the highest absorbance ratio of 0.95 compared to the other samples. On day 1, day 15, and day 30, absolute zeta potential values of -86.58, -83.26, and -80.48 mV were used to validate the results of the absorbance ratio in this sample. Because it has an absolute value of zeta potential in the range of 60-100 mV, this finding classifies the TiO2-POE nanolubricant in sample 6 as a nanolubricant with an excellent level of stability.

The final model utilized in the OFAT analysis was a significant model using analysis of variance (ANOVA). The p-value, which is substantially smaller than 0.05 and is 0.0001, demonstrates this. R^2 are 0.9989 and 0.9999, and the adjusted R^2 value are 0.9983 and 0.9998 respectively,

according to the regression coefficient determined by the analysis of variance. The cubic vs. quadratic model is the best fit for this investigation since it can replicate data reliably and accurately. The absorbance ratios on days 15 and 30 were 0.970918 and 0.949627, respectively. As a result of the uncertainty calculation, these values fall between 0.970918 ± 0.07 and 0.949627 ± 0.09.

Based on OFAT analysis, sample 6 TiO_2-POE nanolubricant is recommended as the ideal sample since it has the most excellent absorbance ratio value of 0.95 with a desirability level of 0.999. Further visual, UV visible spectrophotometry, and absolute zeta potential assessment are recommended to be executed for a more extended period for instance, 1440 or 2160 h, to determine the most extended stability of TiO_2-POE nanolubricant

ACKNOWLEDGMENTS

This study was supported by the Helan Mountain Scholarship program from Ningxia University, China. The authors would like to thank University Malaysia Pahang (UMP) for Grant RDU190336 and the FRGS award RDU 1901112 for financial assistance and facilities provided.

NOMENCLATURE

min	Minute
abs	Absorbance
OFAT	One factor at a time
Std. Dev	Standard deviation
POE	Polyolester
Anova	Analysis of variance
UV	Ultraviolet
A	Initial Absorbance
A_o	Final Absorbance
$\bar{A}_r$	Absorbance Ratio

Greek symbols

ζ	Absolute zeta potential, mV
Ø	Concentration
P	Density

Subscripts

l	Refers to lubricant
p	Refers to nanoparticle

AUTHORSHIP CONTRIBUTIONS

Authors equally contributed to this work.

DATA AVAILABILITY STATEMENT

The authors confirm that the data supporting the study's findings are included in the manuscript.

CONFLICT OF INTEREST

The author declared no potential conflicts of interest with respect to the research, authorship, and/or publication of this article.

ETHICS

There are no ethical issues with the publication of this manuscript

REFERENCES

[1] Choi SU, Eastman JA. Enhancing thermal conductivity of fluids with nanoparticles. Argonne National Lab., IL (United States), 1995.

[2] Kedzierski MA, Gong M. Effect of CuO nanolubricant on R134a pool boiling heat transfer. Int J Refrig 2009;32:791–799. [CrossRef]

[3] Zawawi NNM, Azmi WH, Redhwan AAM, Sharif MZ, Sharma KV. Thermo-physical properties of Al2O3-SiO2/PAG composite nanolubricant for refrigeration system. Int J Refrig 2017;80:1–10. [CrossRef]

[4] Sharif MZ, Azmi WH, Redhwan AAM, Mamat R, Najafi G. Energy saving in automotive air conditioning system performance using SiO2/PAG nanolubricants. J Therm Anal Calorim 2019;135:1285–1297. [CrossRef]

[5] Dhanola A, Garg HC. Experimental analysis on stability and rheological behaviour of TiO2/canola oil nanolubricants. Mater Today Proc 2020;28:1285–1289. [CrossRef]

[6] Mahbubul IM, Elcioglu EB, Amalina MA, Saidur R. Stability, thermophysical properties and performance assessment of alumina–water nanofluid with emphasis on ultrasonication and storage period. Powder Technol 2019;345:668–675. [CrossRef]

[7] Chen Z, Shahsavar A, Al-rashed AAAA, Afrand M. The impact of sonication and stirring durations on the thermal conductivity of alumina-liquid paraffin nanofluid : An experimental assessment. Powder Technology 2020;360:1134–1142. [CrossRef]

[8] Adelekan DS, Ohunakin OS, Babarinde TO, Odunfa MK, Leramo RO, Oyedepo SO, Badejo D C. Experimental performance of LPG refrigerant charges with varied concentration of TiO2nanolubricants in a domestic refrigerator. Case Stud Therm Eng 2017;9:55–61. [CrossRef]

[9] Sharif MZ, Azmi WH, Redhwan AAM, Mamat R. Investigation of thermal conductivity and viscosity of Al2O3/PAG nanolubricant for application in automotive air conditioning system. Int J Refrig 2016;70:93–102. [CrossRef]

[10] Redhwan AAM, Azmi WH, Sharif MZ, Mamat R, Samykano M, Najafi G. Performance improvement

in mobile air conditioning system using Al2O3/PAG nanolubricant. J Therm Anal Calorim 2019;135:1299–1310. [CrossRef]

[11] Ravisankar R, Venkatachalapathy VSK, Alagumurthi N. Application of nanotechnology to improve the performance of tractor radiator using Cu-water nanofluid. J Thermal Eng 2018;4:2188–2200. [CrossRef]

[12] Madani K, Maad RB, Abidi–Saad A. Numerical investigation of cooling a ribbed microchannel using nanofluid. J Therm Eng 2018;4:2408–2422. [CrossRef]

[13] Santos HM, Capelo JL. Trends in ultrasonic-based equipment for analytical sample treatment. Talanta 2007;73:795–802. [CrossRef]

[14] Ghadimi A, Metselaar IH. The influence of surfactant and ultrasonic processing on improvement of stability, thermal conductivity and viscosity of titania nanofluid. Exp Therm Fluid Sci 2013;51:1–9. [CrossRef]

[15] Capelo JL, Maduro C, Vilhena C. Discussion of parameters associated with the ultrasonic solid-liquid extraction for elemental analysis (total content) by electrothermal atomic absorption spectrometry. An overview. Ultrason Sonochem 2005;12:225–232. [CrossRef]

[16] Caneba GT, Dutta C, Agrawal V, Rao M. Novel ultrasonic dispersion of carbon nanotubes. J Miner Mater Charact Eng 2010;9:165–181. [CrossRef]

[17] Nabil MF, Azmi WH, Hamid KA, Mamat R. Experimental investigation of heat transfer and friction factor of TiO2-SiO2 nanofluids in water:ethylene glycol mixture. Int J Heat Mass Transf 2018;124:1361–1369. [CrossRef]

[18] Yashawantha KM, Vinod AV. Experimental investigation on thermal conductivity and stability of water-graphite nanofluid. J Therm Eng 2021;7:1743–1751. [CrossRef]

[19] Nugroho A, Bo Z, Mamat R, Azmi WH, Najafi G, Khoirunnisa F. Extensive examination of sonication duration impact on stability of Al2O3-Polyol ester nanolubricant. Int Commun Heat Mass Transf 2021;126:105418. [CrossRef]

[20] Madderla S, Ramasamy D, Sudhakar K, Kadirgama K, Harun WSW. Heat transfer performance of a radiator with and without louvered strip by using Graphene-based nanofluids. J Therm Eng 2021;7:1315–1328. [CrossRef]

[21] Al-Anssari S, Wang S, Barifcani A, Lebedev M, Iglauer S. Effect of temperature and SiO2 nanoparticle size on wettability alteration of oil-wet calcite. Fuel 2017;206:34–42. [CrossRef]

[22] Al-Anssari S, Arif M, Wang S, Barifcani A, Lebedev M, Iglauer S. Wettability of nanofluid-modified oil-wet calcite at reservoir conditions. Fuel 2018;211:405–414. [CrossRef]

[23] Dagdevir T, Ozceyhan V. Optimization of process parameters in terms of stabilization and thermal conductivity on water based TiO2 nanofluid preparation by using Taguchi method and Grey relation analysis. Int Commun Heat Mass Transf 2021;120:105047. [CrossRef]

[24] Ilyas SU, Ridha S, Abdul Kareem FA. Dispersion stability and surface tension of SDS-Stabilized saline nanofluids with graphene nanoplatelets. Colloids Surf A Physicochem Eng Asp 2020;592:124584. [CrossRef]

[25] Walvekar R, Zairin DA, Khalid M, Jagadish P, Mubarak NM, Tcsm G. Stability, thermo-physical and electrical properties of naphthenic/POME blended transformer oil nanofluids. Therm Sci Eng Prog 2021;23:100878. [CrossRef]

[26] Graves JE, Latvytė E, Greenwood A, Emekwuru NG. Ultrasonic preparation, stability and thermal conductivity of a capped copper-methanol nanofluid. Ultrason Sonochem 2019;55:25–31. [CrossRef]

[27] Arasu VA, Kumar DD, Khan IA. Experimental validation of enhancement in thermal conductivity of titania/water nanofluid by the addition of silver nanoparticles. Int Commun Heat Mass Transf 2021;120:104910. [CrossRef]

[28] Keshvardoostchokami M, Majidi M, Zamani A, Liu B. Adsorption of phenol on environmentally friendly Fe3O4/ chitosan/ zeolitic imidazolate framework-8 nanocomposite: Optimization by experimental design methodology. J Mol Liq 2021;323:115064. [CrossRef]

[29] Rothan, YA, Ali FF, Issakhov A, Selim MM, Li Z. Optimization analysis of hydrogen production using ammonia decomposition. J Mol Liq 2021;335:116190. [CrossRef]

[30] Doube M, Klosowski MM, Arganda-Carreras I, Cordelieres FP, Dougherty RP, Jackson JS, et al. BoneJ: Free and extensible bone image analysis in ImageJ. Bone 2010;47:1076–1079. [CrossRef]

[31] Chen Y, Yu Q, Xu C. A convenient method for quantifying collagen fibers in atherosclerotic lesions by ImageJ software. Int J Clin Exp Med 2017;10:14904–14910.

[32] Rueden CT, Schindelin J, Hiner MC, DeZonia BE, Walter AE, Arena ET, et al. ImageJ2: ImageJ for the next generation of scientific image data. BMC Bioinform 2017;18:529. [CrossRef]

[33] Cai Z, Chattopadhyay N, Liu WJ, Chan C, Pignol JP, Reilly RM. Optimized digital counting colonies of clonogenic assays using ImageJ software and customized macros: Comparison with manual counting. Int J Radiat Biol 2011;87:1135–1146. [CrossRef]

[34] Sharif M, Azmi W, Redhwan A, Mamat R. Investigation of thermal conductivity and viscosity of Al2O3/PAG nanolubricant for application

in automotive air conditioning system. Int J Refrig 2016;70:93–102. [CrossRef]

[35] Ali MKA, Xianjun H. Colloidal stability mechanism of copper nanomaterials modified by ionic liquid dispersed in polyalphaolefin oil as green nano-lubricants. J Colloid Interface Sci 2020;578:24–36. [CrossRef]

[36] Hou X, Jiang H, Ali MKA, Liu H, Su D, Tian Z. Dispersion behavior assessment of the molybdenum disulfide nanomaterials dispersed into poly alpha olefin. J Mol Liq 2020;311:11303. [CrossRef]

[37] Du M, Tang GH. Optical property of nanofluids with particle agglomeration. Solar Energy 2015;122:864–872. [CrossRef]

[38] Tiwari AK, Pandya NS, Said Z, Chhatbar SH, Al-Turki YA, Patel AR. 3S (Sonication, surfactant, stability) impact on the viscosity of hybrid nanofluid with different base fluids: An experimental study. J Mol Liq 2021;329:115455. [CrossRef]

[39] Sarsam WS, Amiri A, Shanbedi M, Kazi SN, Badarudin A, Yarmand H, et al. Synthesis, stability, and thermophysical properties of aqueous colloidal dispersions of multi-walled carbon nanotubes treated with beta-alanine. Int Commun Heat Mass Transf 2017;89:7–17. [CrossRef]

[40] Zawawi NNM, Azmi WH, Sharif MZ, Najafi G. Experimental investigation on stability and thermophysical properties of Al2O3–SiO2/PAG nanolubricants with different nanoparticle ratios. J Therm Anal Calorim 2019;135:1243–1255. [CrossRef]

[41] Shah SNA, Shahabuddin S, Sabri MFM, Salleh MFM, Ali MA, Hayat N, et al. Experimental investigation on stability, thermal conductivity and rheological properties of rGO/ethylene glycol based nanofluids. Int J Heat Mass Transf 2020;150:118981. [CrossRef]

[42] Mahbubul IM, Shahrul IM, Khaleduzzaman SS, Saidur R, Amalina MA, Turgut A. Experimental investigation on effect of ultrasonication duration on colloidal dispersion and thermophysical properties of alumina–water nanofluid. Int J Heat Mass Transf 2015;88:73–81. [CrossRef]

[43] Wilson WW, Wade MM, Holman CS, Champlin FR. Status of methods for assessing bacterial cell surface charge properties based on zeta potential measurements J Microbiol Methods 2000;43:153–164. [CrossRef]

[44] Chibowski E, Szcześ A. Zeta potential and surface charge of DPPC and DOPC liposomes in the presence of PLC enzyme. Adsorption 2016;22:755–765. [CrossRef]

[45] Liao DL, Wu GS, Liao BQ. Zeta potential of shape-controlled TiO2 nanoparticles with surfactants. Colloids Surf A Physicochem Eng Asp 2019;348:270–275. [CrossRef]

[46] Kumar V, Kumar A, Chhabra D, Shukla P. Improved biobleaching of mixed hardwood pulp and process optimization using novel GA-ANN and GA-ANFIS hybrid statistical tools. Bioresour Technol 2019;271:274–282. [CrossRef]

[47] Saha SP, Mazumdar D. Optimization of process parameter for alpha-amylase produced by Bacillus cereus amy3 using one factor at a time (OFAT) and central composite rotatable (CCRD) design based response surface methodology (RSM). Biocatal Agric Biotechnol 2019;19:101168. [CrossRef]

[48] Delgarm N, Sajadi B, Azarbad K, Delgarm S. Sensitivity analysis of building energy performance: A simulation-based approach using OFAT and variance-based sensitivity analysis methods. J Build Eng 2018;15:181–193. [CrossRef]

[49] Yahaya YA, Don MM. Flavonoid production by T. lactinea: screening of culture conditions via OFAT and optimization using response surface methodology (RSM). J Korean Soc Appl Biol Chem 2014;57:749–757. [CrossRef]

[50] Bahiraei M, Hosseinalipour SM, Zabihi K, Taheran E. Using neural network for determination of viscosity in water-TiO2 nanofluid. Adv Mech Eng 2015;4:742680. [CrossRef]

[51] Hemmat Esfe M, Hajmohammad MH. Thermal conductivity and viscosity optimization of nano-diamond-Co 3 O 4 /EG (40:60) aqueous nanofluid using NSGA-II coupled with RSM. J Mol Liq 2017;238:545–552. [CrossRef]

[52] Meybodi MK, Naseri S, Shokrollahi A, Daryasafar A. Prediction of viscosity of water-based Al2O3, TiO2, SiO2, and CuO nanofluids using a reliable approach. Chemometr Intell Lab Syst 2015;149:60–69. [CrossRef]

[53] Zheng Y, Shahsavar A, Afrand M. Ultrasonics - Sonochemistry Sonication time efficacy on Fe3 O4-liquid paraffin magnetic nanofluid thermal conductivity : An experimental evaluation. Ultrason Sonochem 2020;64:105004. [CrossRef]

[54] Tiple A, Sinhmar PS, Gogate PR. Improved direct synthesis of TiO2 catalyst using sonication and its application for the desulfurization of thiophene. Ultrason Sonochem 2021;73:105547. [CrossRef]

[55] Wei H, Afrand M, Kalbasi R, Ali HM, Heidarshenas B, Rostami S. The effect of tungsten trioxide nanoparticles on the thermal conductivity of ethylene glycol under different sonication durations: An experimental examination. Powder Technol 2020;374:462–469. [CrossRef]

[56] Mukherjee S, Mishra PC, Chakrabarty S, Chaudhuri P. Effects of sonication period on colloidal stability and thermal conductivity of SiO2–water nanofluid: An experimental ınvestigation. J Clust Sci 2022;33:1763–1771. [CrossRef]